J Therm Anal Calorim (2011) 103:49–57
DOI 10.1007/s10973-010-1072-6

DSC investigation of nanocrystalline TiO_2 powder

Cornelia Marinescu · Ancuta Sofronia · Cristina Rusti · Roxana Piticescu · Viorel Badilita · Eugeniu Vasile · Radu Baies · Speranta Tanasescu

AICAT2010 Special Chapter

Abstract The aim of the article is to investigate the influence of particle size on titanium dioxide phase transformations. Nanocrystalline titanium dioxide powder was obtained through a hydrothermal procedure in an aqueous media at high pressure (in the range 25–100 atm) and low temperature (≤200 °C). The as-prepared samples were characterized with respect to their composition by ICP (inductive coupled plasma), structure and morphology by XRD (X-ray diffraction), and TEM (transmission electron microscopy), thermal behavior by TG (thermogravimetry) coupled with DSC (differential scanning calorimetry). Thermal behavior of nanostructured TiO_2 was compared with three commercial TiO_2 samples. The sequence of brookite–anatase–rutile phase transformation in TiO_2 samples was investigated. The heat capacity of anatase and rutile in a large temperature range are reported.

Keywords TiO_2 · Nanomaterial · Phase transformation · Thermal analysis

C. Marinescu (✉) · A. Sofronia · S. Tanasescu
Institute of Physical Chemistry Ilie Murgulescu of the Romanian Academy, 060021 Bucharest, Romania
e-mail: alcorina@chimfiz.icf.ro

C. Rusti · R. Piticescu · V. Badilita
National Institute of Research and Development for Non-Ferrous and Rare Metals, 077145 Bucharest, Romania

E. Vasile
METAV—Research and Development, 020011 Bucharest, Romania

R. Baies
National Research Institute for Electrochemistry and Condensed Matter, 300224 Timisoara, Romania

Introduction

TiO_2 is a well-known mineral that occurs in three phases: rutile, anatase, and brookite [1], each having different structures. All the three phases have been studied for their high photocatalitic activity, high dielectric, and semi-conducting properties, good biocompatibility, but also due to their potential as catalyst or active supports [2–8]. These properties are different relative to the TiO_2 phases and are closely related to its crystal structure, which makes phase transformation one of the most important issues in practical application of the compound.

Rutile is the most common, stable and well known mineral of the three phases. Anatase and brookite both transform exothermally and irreversibly to rutile upon heating [9]. The transformation sequence and phase stability strongly depend on the initial particle sizes of anatase and/or brookite [10].

In terms of crystal structure, rutile, anatase, and brookite have Ti in an octahedral coordination with respect to O. In all these three crystal structures, Ti^{4+} is present as $[TiO_6]$ octahedra which share edges and corners. In brookite the octahedra share both edges and corners, forming an orthorhombic structure, while anatase and rutile crystallize in a tetragonal unit cell. The number of edges shared by the $[TiO_6]$ octahedra increases from two in rutile to four in anatase. In rutile there are straight chains of octahedra; in anatase zigzag chains [11]. The Ti–O bond angle of every $[TiO_6]$ octahedron is different in the three structures. Therefore, in the phase transformation process from anatase and brookite to rutile a substantial rearrangement of the structure must occur [12, 13].

The temperature of the phase transition anatase to rutile is in the range between 350 and 1175 °C [14]. The brookite–rutile transition mainly proceeds in the temperature

range 500–600 °C [15]. Data regarding the brookite–anatase phase transition is rather scarce. It has been reported that the transformation to rutile is affected by the initial particle size, the method of preparation of the sample, the presence of impurities, or additives for the stabilization of the certain modification, and by the atmosphere present during the transformation [4, 5, 16–22]. There is, however, some ambiguity regarding the sequences of phase transformation of the TiO_2 polymorph phases (anatase, brookite, and rutile) during the heating process. In this article, the stability at high temperature of TiO_2 anatase with different particle size was investigated. The role of the brookite phase in the anatase to rutile transition is also of interest to this study. The heat capacity of anatase and rutile in a large temperature range are reported.

Experimental

Sample preparation

Titanium dioxide (TiO_2) was synthesized in hydrothermal conditions starting from soluble salts of titanium (purity grade >99%) and ammonium chloride as mineralize agent. The aqueous precursor suspension was placed in a Cortest, USA autoclave and hydrothermally treated at high pressures (in the range 25–100 atm) and low temperatures (≤200 °C). After the reaction was completed, the as resulted powder was filtered, washed several times with distilled water, and dried in an oven at 100 °C.

Methods and measurements

The nanostructured titanium dioxide thus obtained was characterized from the point of view of composition by inductively coupled plasma analysis (ICP; Spectroflame equipment) and microstructure by X ray diffraction analysis (XRD Bruker D8 Advance diffractometer endowed with DIFFRAC^{plus} BASIC Evaluation Package, version EVA12, 2006 soft and data base ICDD PDF-2 Release 2006).

The sample was morphologically examined by transmission electron microscopy in the bright field (TEMBF), selected area electron diffraction (SAED), and high resolution transmission electron microscopy (HRTEM), using TECNAI F30 G2 equipment, with a linear resolution of 1 Å.

For the thermal characterization a simultaneous high temperature thermogravimetry (TG) and differential scanning calorimetry (DSC) was employed. Thermal properties (temperature and enthalpies of transformation, heat capacity, and mass change) of the TiO_2 samples were measured by a TG-DSC Setaram Setsys Evolution 17 analyzer, in the temperature range from room temperature to 1200 °C. Sample mass for simultaneous TG-DSC measurements was cca 20 mg and for heat capacities measurements of about 100 mg.

The thermo analyzer calibration was performed using standard metallic substances in the whole temperature range of the experiment, with 5, 10, and 15 °C/min heating rates, with the same type of crucible used for experiments (alumina crucibles) and with the same carrier gas (Ar with high purity). The onset melting point temperatures and heats of fusion of 99.99% purity standard metallic materials (In, Sn, Pb, Zn, Al, Ag, and Au), were used for temperature correction and energy calibration.

Heat capacities were determined by performing three consecutive experiments in identical conditions, namely the same heating rate (10 °C/min), same gas flow, Ar, at a rate of 16 ml/min, Pt crucibles. The method consists in performing three runs with two vessels: the measuring and the reference vessel. The first run is done with the two empty vessels (blank test), the second run with reference material with a known heat capacity C_p (in our experiments—sapphire) and the third run with sample. Each run consist in a ramp between in the initial temperature and the final temperature, at a constant heating rate of 10 °C/min. Experimental heat capacity was determined for two temperature ranges: 300–800 and 750–1200 °C.

To calculate peak temperatures, peak's area and heat capacities (Calisto–AKTS) instruments' software was used.

Results and discussion

Composition

All the samples were investigated for impurities by ICP. Samples have a purity of 99%.

Morphological and structural characterization

XRD characterization

The hydrothermal prepared sample, characterized by X-ray diffraction as a mixture of 88% anatase and 12% brookite (Fig. 1) was compared to commercial TiO_2 samples (Table 1).

In Fig. 1 is presented the difractogram for a representative S1-A, B sample.

Graphical representation of the results by the FPM (Full pattern matching) method consists of:

- Experimentally measured difractogram (black dotted line; sample);

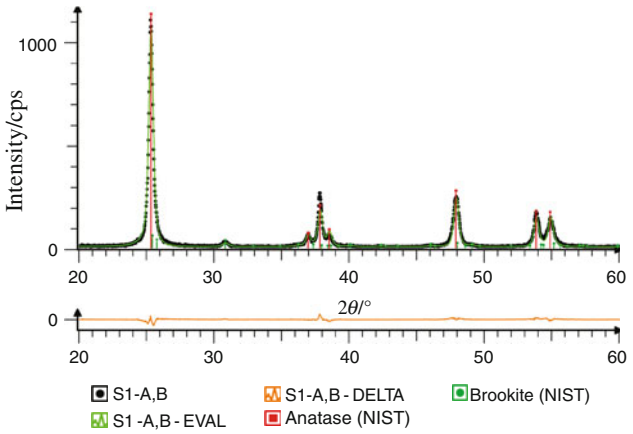

Fig. 1 Graphic representation of the results obtained by FPM method for XRD quantitative phase analysis for S1-A, B sample (anatase (NIST) -03-065-5714 (*) and brookite (NIST) -03-065-2448 (I))

Table 1 Samples composition and crystallite sizes from X-ray measurements

Sample	Sample provenience	% TiO_2 phase composition and crystallite size
S1–A, B[a]	Hydrothermal synthesis	A 88%: 21.7 nm
		B 12%: 14.6 nm
S2-A, R[a]	Commercial	A 98.2%: 87.7 nm
		R 1.8%: 91.9 nm
S3-A	Commercial	A: 74.8 nm
S4-R	Commercial	R: 106.0 nm

[a] *A* anatase, *B* brookite, *R* rutile

- Evaluation difractogram (green; sample-EVAL), obtained by simulation;
- The diference between the two previous difractograms (orange; sample-DELTA), for evidentiating the simulating quality;
- Sticks difractograms for compounds that are taken into consideration (identified), according to the PDF references.

Commercially available anatase and rutile mixture (S2-A, R sample), anatase (S3-A), and rutile (S4-R) TiO_2 were also characterized for comparison with the hydrothermal synthesized sample (S1-A, B). From X-ray measurements (Figs. 1, 2, 3) the crystallite size of the TiO_2 phases were determined (Table 1). Quantitative evaluation and crystallographic characterization of the identified phases was made with the help of the FPM module (contained within the DIFFRAC^{plus} BASIC (Bruker AXS) program package).

For the S4-R sample a very pronounced preferential increasing of the commercial rutile crystals on [110] direction was observed, for this reason the FMP method

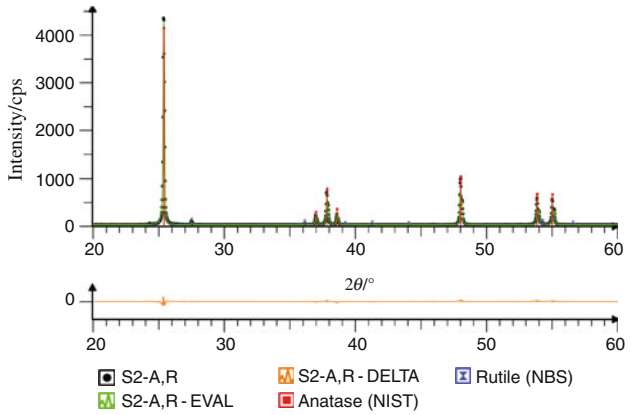

Fig. 2 Graphic representation of the results obtained by FPM method for XRD quantitative phase analysis for S2-A, R sample (Anatase (NIST) -03-065-5714 (*); Rutile (NBS) -00-021-1276 (*))

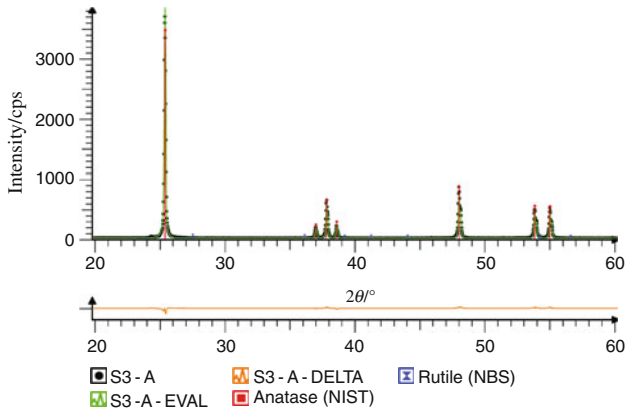

Fig. 3 Graphic representation of the results obtained by FPM method for XRD quantitative phase analysis for S3-A sample (Anatase (NIST) -03-065-5714 (*)

cannot be applied. However, the semi-quantitative composition could be estimated.

The criteria used for comparing the simulated difractogram with that measured are the mean reliability R_{WP}:

$$R_{WP} = \sqrt{\frac{\sum_i w_i x[y_i^{obs} - y_i^{calc}]^2}{\sum_i w_i x y_i^{obs^2}}} \times 100\%$$

Other criteria that characterized inevitable discrepancy due to counting statistics R_0 is:

$$R_0 = \sqrt{\frac{\sum_i w_i x y_i^{obs}}{\sum_i w_i x y_i^{obs^2}}} \times 100\%$$

in which: y_i^{obs} intensity in point i from the measured difractogram, y_i^{calc} intensity in point i from the simulated pictogram, w_i mean factor.

Table 2 Lattice parameters of TiO_2 samples

Sample	TiO_2 phase	System	Space group	Z/formula units per cell	Cell param./Å			Cell volume	Theoretical density/ g cm^{-3} [21]	Experimental density/g cm^{-3}
					a	*b*	*c*			
S1-A, B	Anatase	Tetragonal	I41/amd (141)	4	3.79211	3.79211	9.50566	136.69232	3.90	3.88
	Brookite	Orthorhombic	Pbca (61)	8	9.18500	5.44700	5.14500	257.40792	4.13	4.12
S2-A, R	Anatase	Tetragonal	I41/amd (141)	4	3.78508	3.78508	9.51311	136.29271	3.90	3.89
	Rutile	Tetragonal	P42/mnm (136)	2	4.59376	4.59376	2.95850	62.43231	4.27	4.25
S3-A	Anatase	Tetragonal	I41/amd (141)	4	3.78481	3.78481	9.51354	136.27943	3.90	3.89
S4-R	Rutile	Tetragonal	P42/mnm (136)	2	4.59395	4.59395	2.95910	62.44996	4.27	4.25

The ratio R_{WP}/R_0 defines the relative reliability and tends to one for a perfect fitting. The relative reliability value for S1-A, B; S2-A, R; and S3-A samples is about 1.67. Lattice parameters of the samples refined by the Rietveld refinement method are presented in Table 2.

TEM (HRTEM) characterization

For morphological characterization of TiO_2 powder, small quantities of sample were immersed in ethylic alcohol. The suspension was then homogenized in an ultrasonic bath. Fine particles from the resulted suspension were selected using a copper grid covered with FORMVAR and examined by transmission electron microscopy in the bright field (TEMBF), selected area electron diffraction (SAED), and high resolution transmission electron microscopy (HRTEM).

Electron diffraction image (SAED) in Fig. 5 obtained on a nanoarea of Fig. 4 is typical of a nanocrystalline phase with randomly oriented small crystallites. Outlined circles correspond to the interplanar distances specified in the left corner of the image Fig. 5.

The interplanar distances corresponding crystalline planes visible in Fig. 6 obtained by Fourier transform (Fig. 7) have the following values: 1,2A; 1,3A; 1,5A; 2A; and 2,1A.

TEM analysis reveals that the particles are quasi-spheres and are quite uniform in their overall morphology.

Thermal analysis

Thermal analysis is the study of the relationship between a sample property and its temperature as the sample is heated or cooled in a controlled manner [23]. In this article, thermal analysis refers to differential scanning calorimetry (DSC) and thermogravimetry (TG). Differential scanning calorimetry is a technique used to determine the heat flow in and out of a sample when subjected to a temperature pro-

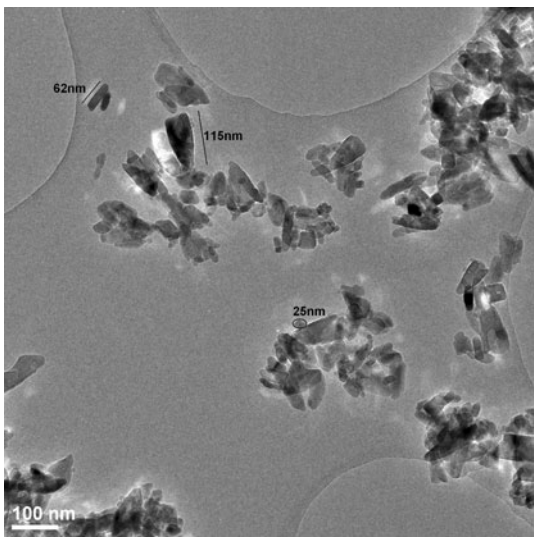

Fig. 4 Bright field TEM image. Aggregate of nanoparticles

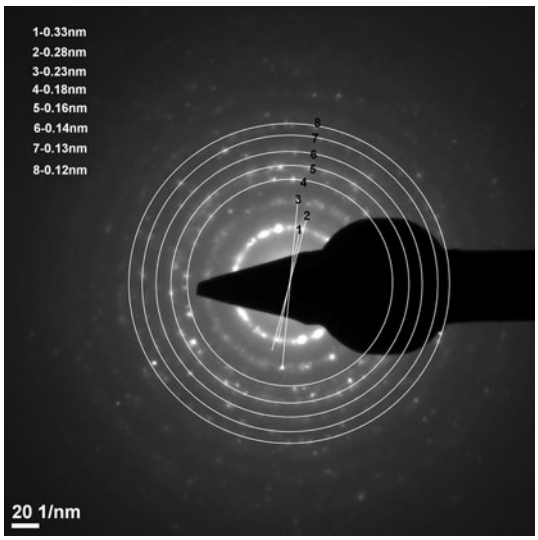

Fig. 5 Electron diffraction image (SAED) associated with the area of Fig. 4

gram in a controlled atmosphere. When heating or cooling a sample, thermal changes in a material are accompanied by an exchange of heat; hence the temperature of these transformations and heat flow can be determined. Thermogravimetry follows the mass changes in a sample subjected to thermal treatment. A thermogravimetric analysis can be recorded as a change in sample mass with temperature and time, and with pressure and gas composition.

These techniques are widely employed to provide qualitative, semi-quantitative, and in some cases quantitative measurements of the energetic evolution materials on heating or cooling over a considerable temperature range [24].

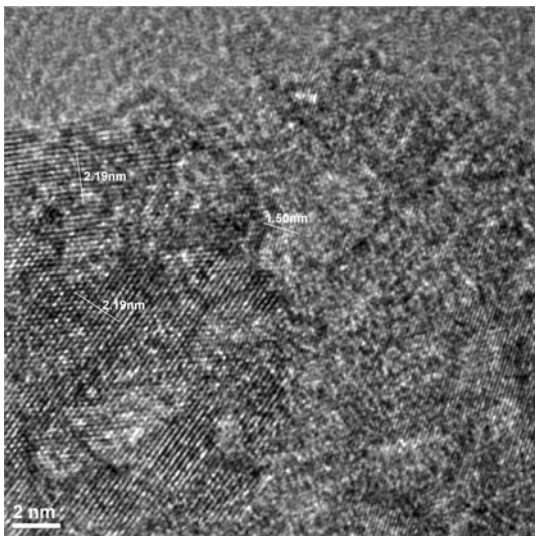

Fig. 6 HRTEM image of TiO_2 nanoparticles at high magnification

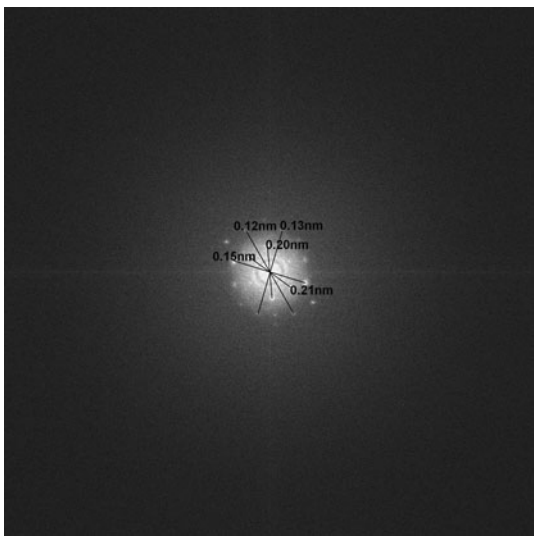

Fig. 7 Fast Fourier transform (FFT) corresponding Fig. 6

Brookite transformation study

DSC measurements of the S1-A, B sample were done with three heating rates of 5, 10, and 15 °C/min (Fig. 8).

To investigate the sequences of phase transformation of the S1-A, B sample (mixture of 88% anatase and 12% brookite) during the heating process at the 10 °C/min heating rate in a large temperature range (40–1100 °C), the X-ray measurements have been performed at different stages corresponding to thermal events observed on the DSC curve. In Fig. 8 the following aspects can be revealed:

– Up to 600 °C an exothermic effect without a clear peak can be observed; it corresponds to the decrease in the mass fraction of brookite content without the formation of rutile phase, obtaining a mixture of 96.13% anatase and 3.87% brookite with crystallite size of 24 and 16 nm, respectively. At this stage, the cell parameters of brookite ($a = 9.17917$, $b = 5.42026$, $c = 5.13299$) remain almost unchanged, while those of anatase, both a and c ($a = 3.77906$, $c = 9.48536$) slowly decrease, therefore the growth rates in all the crystallographic planes are similar. However, there is no detectable amount of rutile phase in the sample. Up to 600 °C, 33.33% of the initial phase of brookite transformed into anatase at a low conversion rate, without any clear peak associated with transformation on the DSC curve being detected. At the same time with brookite transformation, particles growth takes place. The growth rates of the particles of these two phases are almost equal at $T < 600$ °C, anatase particle growing by 2.3 nm and brookite particle by 1.4 nm. On heating at $T > 600$ °C, the growth rate of the particles increases and the remaining brookite phase transforms to anatase (Fig. 9) and subsequently anatase to rutile (Fig. 11).

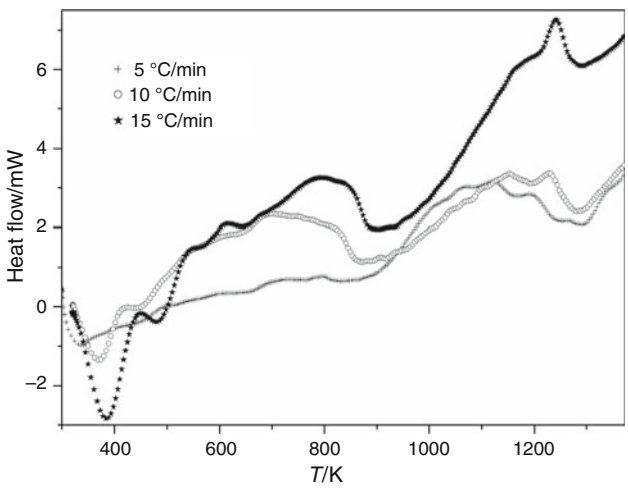

Fig. 8 Heat flow curves of the S1-A, B sample at 5, 10, and 15 °C/min heating rates

– Above 600 °C the brookite–anatase transformation take place in a narrow temperature range between 600 and 725 °C with a maximum rate at the 680 °C, visible transformation on heat capacity curve (Fig. 9). The brookite–anatase transition is completed at 800 °C when single phase anatase with a crystallite size of 69.7 nm is observed in the X-ray diffraction pattern. Bokhimia and Pedraza [25] pointed out that the transformation of brookite and anatase phases into rutile occurs above 800 °C, in good agreement with our experimental results.

The influence of the heating rate on the phase transformation behavior was also a part of this study. The brookite–anatase transformation is shifted to a higher temperature range when a slow heating rate of 5 °C/min is used (Fig. 8). Zhang and Banfield [16, 17] pointed out that the stability of TiO_2 polymorphs is crystallite size dependent: anatase is most stable at <11 nm, optimum brookite crystallite size being between 11 and 35 nm, while rutile is favored at sizes greater than 35 nm. Zhang and Banfield [16] also predicted reversible transformations between anatase and brookite in certain size domains (brookite size <11 nm and anatase size >11 nm) where brookite and anatase are metastable. The hydrothermal synthesized TiO_2 (S1-A, B sample) has crystallite size of brookite phase of 14.6 nm in the brookite stable region; also, the brookite phase transformation is not reversible, no thermal effect on the DSC cooling curve was observed. As a consequence of the thermodynamic stability and the activation energy dependence of the crystallite size [26–28], the brookite phase of S1-A, B sample is thermodynamically stable and the phase transition does not begin when heating until the critical particle size and the activation energy are reached. Xisheng Ye et al. [29] pointed out that the grain growth rate is small in the range below 780 °C. For the heating rate of 5 °C/min, in the temperature range of rutile transition, 800–1000 °C, it is likely that the structural phase transitions brookite to anatase and anatase to rutile co-exist. The lowest transition temperature to rutile and the greatest transition enthalpy obtained for the heating rate of 5 °C/min support the above observation (Table 3).

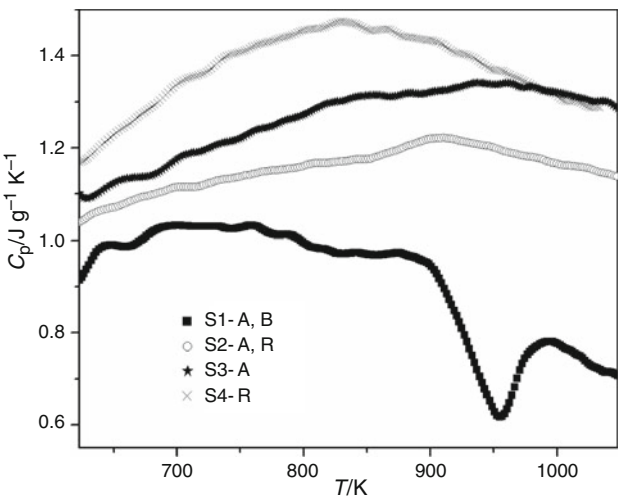

Fig. 9 Heat capacity curves of TiO_2 samples in the temperature range of 350–800 °C

The thermal effect of the irreversible transformation to rutile is more evident with the increasing of heating rate and the transition point is shifted to higher temperatures (Fig. 8). Table 3 presents the rutile transformation peak temperatures, T_p, and transformation energies at different heating rates for S1-A, B sample.

The detection of a small fraction of brookite and no rutile phase at 600 °C and only anatase phase at 800 °C mean that the sequence of the phase transitions of the mixture of 21.7 nm anatase (88%) and 14.6 nm brookite (12%) is: brookite → anatase → rutile.

Anatase transformation study

As the presence of TiO_2 anatase or rutile phases is critical for the properties of the materials used in applications [2–8], many researchers tried to understand and control the anatase–rutile transition.

Crystallite size is one of the most important factors to control the phase stability of TiO_2 polymorph phases [16]. In Fig. 10 the DSC curve of the hydrothermal prepared (S1-A, B) sample together the DSC curves of the S2-A, R sample (a mixture of anatase and 1.8% rutile), the S3-A sample (a singular anatase phase), and the S4-R sample (a single rutile phase), respectively, are shown for comparison. The corresponding crystallite sizes are those presented in the Table 4.

The presence of 12% brookite in the S1-A, B sample accelerates the transition to rutile, and in the same time, anatase with the 21.7 nm crystallite size not in it stability domain will also contribute at a lower transition temperature. The existence of brookite, therefore, is responsible for the enhancement of the anatase to rutile transition.

However, the variation in the transition point is more evident from the heat capacity curves (Fig. 11). To better reflect the phase transformation to rutile, heat capacity

Table 3 The rutile transformation peak temperatures, T_p, and transformation energies of S1-A, B sample at different heating rates

Heating rate/degree min^{-1}	T_{peak}/°C	Transformation energy/kJ mol^{-1}
5	929	−0.7147854
10	963	−0.6332075
15	969	−0.4950604

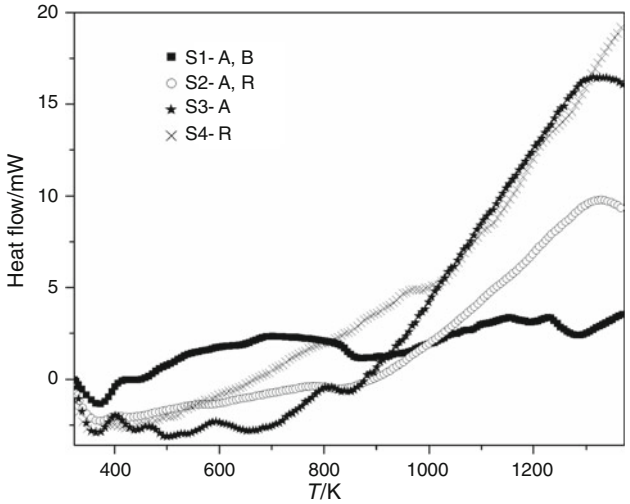

Fig. 10 DSC curves of TiO_2 samples at heating rate of 10 °C/min

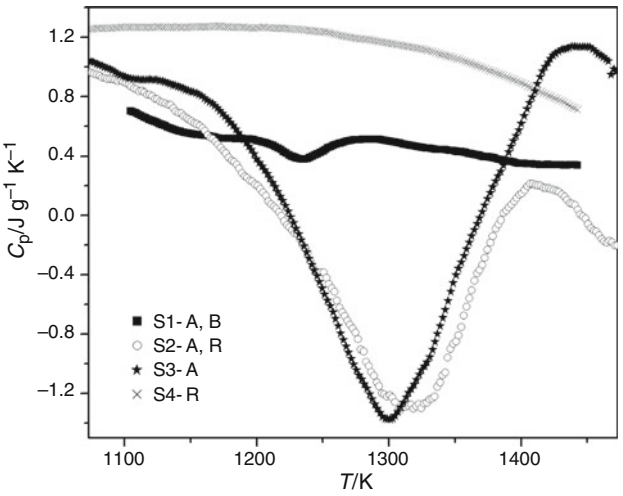

Fig. 11 Comparative C_p curves of TiO_2 samples at the heating rate of 10 °C/min

Table 4 Comparative rutile transformation peak temperatures, T_p at heating rate of 10°/min, determinate from C_p curves

Sample	T_p/°C	Initial crystallite size/nm	Final rutile crystallite size
S1-A, B	963	A: 21.7	>1 μm
		B: 14.6	
S2-A, R	1040	A: 87.7	>1 μm
		R: 91.9	
S3-A	1027	A: 74.8	166 nm

measurements were performed in the temperature range of 750–1200 °C.

The anatase-to-rutile transformation in nanocrystalline materials is considerate rate limited by rutile nucleation, as opposed to rutile growth [28]. This could explain the higher transition temperature of the S2-A, R sample which contains a small percentage 1.8% of rutile comparative to anatase single phase sample (S3-A) (Table 4). Since the crystallite sizes of the two anatase phases of the above samples are near each other, the result would be only a small variance in the temperatures of anatase to rutile transition ($\Delta T \cong 13$ °C). Note also that the anatase to rutile transformation occurs with a strong thermal effect, in a wide range of temperature from 800 to 1150 °C, which leads to the conclusion that the anatase to rutile transition takes place along with the growth of the already formed rutile particles.

The temperature dependences of heat capacity for anatase single phase S3-A and rutile single phase S4-R samples was determined. C_p experimental data at high temperatures are not reported in the literature.

Anatase in the temperature range of 623–1050 K:

$$C_p(\text{J/mol K}) = 2.25140 \times 10^3 - 13.18299 \times T + 0.0314 \times T^2 - 3.67965 \times 10^{-5} \times T^3 + 2.14453 \times 10^{-8} \times T^4 - 5.0075 \times 10^{-12} \times T^5$$

$R^2 = 0.99606$

Rutile in the temperature range of 623–1050 K:

$$C_p(\text{J/mol K}) = 1.42549 \times 10^3 - 7.6724 \times T + 0.0157 \times T^2 - 1.35781 \times 10^{-5} \times T^3 + 4.22932 \times 10^{-9} \times T^4$$

$R^2 = 0.99768$

Rutile in the temperature range of 1067–1443 K:

$$C_p(\text{J/mol K}) = 1.36879 \times 10^3 - 3.74221 \times T + 0.00375 \times T^2 - 1.35955 \times 10^{-6} \times T^3 + 8.62422 \times 10^{-11} \times T^4$$

$R^2 = 0.99946$

Water desorption

Taking into account the purity grade of the samples (higher than 99%), the major component associated with the mass loss of the sample is water. The enthalpy difference between a nanocrystalline sample and bulk rutile arises from polymorphism, surface energy, and the presence of water [17]. At high temperatures, TiO_2 nanoparticles dehydrate and coarsen, the final stable phase upon grain growth being always rutile. The overall process (phase transformation, water loss, and coarsening) is irreversible. The TiO_2 samples contain adsorbed water which has the properties of bulk liquid water and a small fraction bound very tightly, probably in the form of hydroxyl groups [30].

Thermogravimetric analysis of TiO_2 powders at the heating rate of 10 °C/min (Fig. 12) shows that mass loss occurs mainly up to 600 °C.

The TG curve of the S1-A, B sample shows that dehydration occurs over a wide range of temperature in two not well defined stages, with maximum rates of desorption of water at 98 and 247 °C. The latter two temperatures are clearly observed on dTG curve (inset of Fig. 12). The thermal event at 98 °C can be correlated to the DSC endothermic peak which was observed near the same temperature. However, for the greatest mass loss that maximizes at 247 °C, there is a sequence of thermal effects corresponding to the DSC curve in the temperature range of 150–400 °C. The endothermic peak occurring below 100 °C corresponds to the weakly adsorbed water removal (0.006 mol of 0.028 mol total water content) and the 1.509% mass loss between 150 and 400 °C being attributed to the decomposition of the hydroxyl group; the OH groups were eliminated as water and the Ti–O–Ti bond was produced [31]. The mass loss that occurs below 400 °C corresponds to desorption of physisorbed water (85% of total mass loss) and the mass loss that occurs above 400 °C confirm the existence of some amount of chemically bound water.

From thermogravimetric measurements the content of water of TiO_2 samples has been calculated. The sample mass was normalized to obtain 1 mol of sample and x moles of water (Table 5). It can be observed that the smallest sample size of particle, having higher surface energy, can adsorb a larger water quantity to the surface.

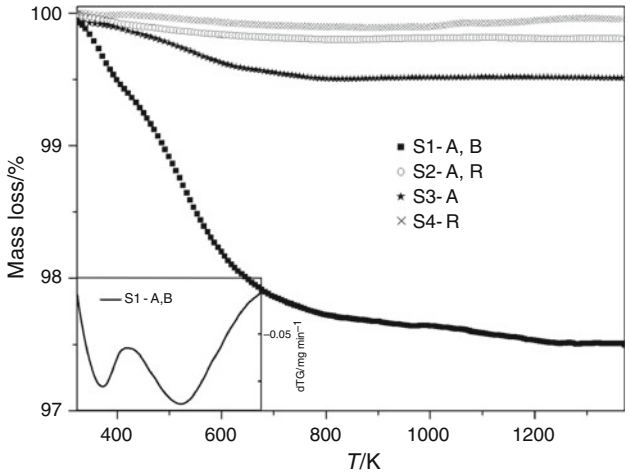

Fig. 12 TG curves of TiO_2 sample

Table 5 Moles of water corresponding to 1 mol of TiO_2 samples

Sample $TiO_2 \cdot xH_2O$	Crystallite size/nm	Weight loss %	x/moles of water
S1-A, B	A: 21.7	2.455	0.11164
	B: 14.6		
S2-A, R	A: 87.7	0.202	0.00890
	R: 91.9		
S3-A	A: 74.8	0.341	0.01520
S4-R	R: 106	0.110	0.00478

Conclusions

The thermal behavior of nanocrystalline TiO_2 powders using thermogravimetry and differential scanning calorimetry analysis in the temperature range from room temperature to 1200 °C has been studied.

Experimental results have shown that the anatase to rutile phase transformation depends not only on primary crystallite size, but also on the presence of the brookite phase and adsorbed water. The presence of the brookite phase accelerates the anatase to rutile transformation. Water desorbs over a wide range of temperature ($T \leq 600$ °C), confirming the existence of some amount of chemically bound water. The brookite–anatase–rutile transformations are thermodynamically favorable in the large temperature range of 200–1150 °C.

The obtained results will be further used for preparing single phase nanostructured anatase powders in hydrothermal conditions for save energy applications.

Acknowledgements The financial support of the National Program II—IDEAS no. 50/2007-2010 Grant and National Program II—Partnership ctr 72-184 are acknowledged.

References

1. Wells AF. Structural inorganic chemistry. 4th ed. Oxford: Clarendon Press; 1975.
2. Dagan G, Tomkiewicz M. Titanium dioxide aerogels for photocatalytic decontamination of aquatic environments. J Phys Chem. 1993;97:12651–5.
3. Wei ZB, Yan W, Zhang H, Ren T, Xin Q, Li Z. Hydrodesulfurization activity of NiMo/TiO2#Al2O3 catalysts. Appl Catal A Gen. 1998;167:39–48.
4. Zhang HZ, Banfield JF. Thermodynamic analysis of phase stability of nanocrystalline titania. J Mater Chem. 1998;8:2073–6.
5. Gribb AA, Banfield JF. Particle size effects on transformation kinetics and phase stability in nanocrystalline TiO $_2$. Am Mineral. 1997;82:717–28.
6. Matos BR, Aricó EM, Linardi M, Ferlauto AS, Santiago EI, et al. Thermal properties of Nafion–TiO_2 composite electrolytes for PEM fuel cell. J Therm Anal Calorim. 2009;97(2):591–4.
7. Madarász J, Brăileanu A, Crişan M, Răileanu M, Pokol G. Evolved gas analysis of amorphous precursors for S-doped TiO_2 by TG-FTIR and TG/DTA-MS.Part 3. Candidate from thiourea and Ti(IV)-ethoxide. J Therm Anal Calorim. 2009;97(1):265–71.
8. Crişan M, Brăileanu A, Crişan D, Răileanu M, Drăgan N, et al. Thermal behaviour study of some sol-gel TiO_2 based materials. J Therm Anal Calorim. 2008;92(1):7–13.
9. Greenwood, Norman N, Earnshaw A. Chemistry of the elements. Oxford: Pergamon; 1984.

10. Riedel R, Wei I, editors. Ceramics science and technology: properties, vol. 2. Weinheim: Wiley-VCH Verlag GmbH & Co. KGaA; 2010.
11. Heald EF, Weiss CW. Kinetics and mechanism of the anatase/rutile transformation, as catalyzed by ferric oxide and reducing conditions. Am Mineral. 1972;57:10–23.
12. Wang Z, Deng X. Al2O3 composite agent effects on phase transformation of nanometer TiO2 powder. Mater Sci Eng B. 2007;140:109–13.
13. Huberty J, Xu H. Kinetics study on phase transformation from titania polymorph brookite to rutile. J Solid State Chem. 2008;181:508–14.
14. Daβler A, Feltz A, Jung J, Ludwig W, Kaisersberger E. Characterization of rutile and anatase powders by thermal analysis. J Therm Anal Calorim. 1988;33:803–9.
15. Li J-G, Ishigaki T. Brookite → rutile phase transformation of TiO2 studied with monodispersed particles. Acta Mater. 2004;52:5143–50.
16. Zhang HZ, Banfield JF. Understanding polymorphic phase transformation behavior during growth of nanocrystalline aggregates: insights from Tio_2. J Phys Chem B. 2000;104:3481–7.
17. Ranade MR, Navrotsky A, Zhang HZ, Banfield HZ, Elder SH, Zaban A, Borse PH, Kulkarni SK, Doran GS, Whitfield HJ. Energetics of nanocrystalline TiO2. Proc Natl Acad Sci USA. 2002;99(2):6476–81.
18. Yoganarasimhan SR, Rao CNR. Mechanism of crystal structure transformations. Part 3.—factors affecting the anatase-rutile transformation. Trans Faraday Soc. 1962;58:1579–89.
19. Shannon RD, Pask JA. Kinetics of the anatase-rutile transformation. J Am Ceram Soc. 1965;48:391–8.
20. Gennari FC, Pasquevich DM. Kinetics of the anatase–rutile transformation in TiO2 in the presence of Fe2O3. J Mater Chem. 1998;33:1571–8.
21. Arbiol J, Cerda J, Dezanneau G, Cirera A, Peiro F, Cornet A, Morante JR. Effects of Nb doping on the TiO_2 anatase-to-rutile phase transition. J Appl Phys. 2002;92:853–61.
22. Burns A, Hayes G, Li W, Hirvonen J, Demaree JD, Shah SI. Neodymium ion dopant effects on the phase transformation in sol–gel derived titania nanostructures. Mater Sci Eng B. 2004;111:150–5.
23. Gallagher PK. Handbook of thermal analysis and calorimetry vol. 5: Recent advances techniques and applications. In: Brown ME, Gallagher PK, editors; 2008.
24. Navrotsky A. Thermochemistry of nanomaterials. Rev Miner Geochem. 2001;44:73–103.
25. Bokhimia X, Pedrazab F. Characterization of brookite and a new corundum-like titania phase synthesized under hydrothermal conditions. J Solid State Chem. 2004;177:2456–63.
26. Zhang HZ, Banfield JF. Phase transformation of nanocrystalline anatase-to-rutile via combined interface and surface nucleation. J Mater Res. 2000;15:437–48.
27. Tanaka K, Iwama S, Mihama K. Crystallization of nanometer–sized amorphous sb particles formed by flowing gas evaporation technique. Jpn J Appl Phys. 1998;37:L669–71.
28. Celine Perego, Renaud Revel, Olivier Durupthy, Sophie Cassaignon, Jean-Pierre Jolivet. Thermal stability of TiO_2-anatase: impact of nanoparticles morphology on kinetic phase transformation. Solid State Sci. 2010;12:989–95.
29. Ye X, Sha J, Jiao Z, Zhang L. Thermoanalytical characteristic of nanocrystalline brookite-based titanium dioxide. NanoStruct Mater. 1997;8(7):919–27.
30. Madras G, McCoy BJ, Navrotsky A. Kinetic model for TiO2 polymorphic transformation from anatase to rutile. J Am Ceram Soc. 2007;90:250–5.
31. Nakayama N, Hayashi T. Preparation of TiO_2 nanoparticles surface-modified by both carboxylic acid and amine: Dispersibility and stabilization in organic solvents. Colloids Surf A Physicochem Eng Asp. 2008;317:543–50.